ground water

Delineating Alluvial Aquifer Heterogeneity Using Resistivity and GPR Data

by Jerry C. Bowling[1], Antonio B. Rodriguez[2], Dennis L. Harry[3], and Chunmiao Zheng[2]

Abstract

Conceptual geological models based on geophysical data can elucidate aquifer architecture and heterogeneity at meter and smaller scales, which can lead to better predictions of preferential flow pathways. The macrodispersion experiment (MADE) site, with >2000 measurements of hydraulic conductivity obtained and three tracer tests conducted, serves as an ideal natural laboratory for examining relationships between subsurface flow characteristics and geophysical attributes in fluvial aquifers. The spatial variation of hydraulic conductivity measurements indicates a large degree of site heterogeneity. To evaluate the usefulness of geophysical methods for better delineating fluvial aquifer heterogeneities and distribution of preferential flow paths, a surface grid of two-dimensional ground penetrating radar (GPR) and direct current (DC) resistivity data were collected. A geological model was developed from these data that delineate four stratigraphic units with distinct electrical and radar properties including (from top to bottom) (1) a meandering fluvial system (MFS); (2) a braided fluvial system (BFS); (3) fine-grained sands; and (4) a clay-rich interval. A paleochannel, inferred by other authors to affect flow, was mapped in the MFS with both DC resistivity and GPR data. The channel is 2 to 4 m deep and, based on resistivity values, is predominantly filled with clay and silt. Comparing previously collected hydraulic conductivity measurements and tracer-plume migration patterns to the geological model indicates that flow primarily occurs in the BFS and that the channel mapped in the MFS has no influence on plume migration patterns.

Introduction

Quantifying the flow and transport properties of aquifer systems is a fundamental but challenging aspect of ground water remediation and typically revolves around adequate characterization of the three-dimensional (3D) hydraulic conductivity field. In clastic braided fluvial aquifers, hydraulic conductivity is closely related to lithology and the stratigraphic architecture of the aquifer. Fluvial aquifers are particularly challenging because they involve a mixture of grain sizes ranging from gravel to clay, a broad range of grain-size sorting ranging from poorly sorted to nearly homogeneous facies, and a broad range of interconnectivity between lithostratigraphic facies at scales ranging from tens of meters (e.g., channel fill) to centimeters (e.g., flaser bedding). Quantification of hydrological attributes tends to rely heavily on one-dimensional measurements such as borehole data (e.g., flow monitoring, geophysical and lithologic logs, and sediment cores). In contrast, surface geophysical methods (i.e., radar, electrical, and seismic methods) provide dense spatial coverage, albeit with only indirect links to hydrological attributes such as hydraulic conductivity, porosity, or pore fluid type. However, a qualitative and occasionally quantitative relationship can often be found between geophysical methods and hydrological attributes, particularly in regards to estimating lithology and hydraulic conductivity from resistivity data (e.g., Heigold et al. 1979; Kosinski and Kelly 1981; Urish 1981; Ponzini et al. 1984; Frohlich et al. 1996). Geophysical studies may therefore contribute to producing an overall better subsurface model for ground water flow and contaminant transport. Electrical resistivity and ground penetrating radar (GPR), in particular, have become popular geophysical methods for characterizing subsurface

[1]Corresponding author: BP America Inc., 200 Westlake Park Blvd., Houston, TX 77079; (281) 366-6257; Jerry.Bowling@bp.com
[2]Department of Geological Sciences, University of Alabama, P.O. Box 870338, Tuscaloosa, AL 35487-0339.
[3]Department of Geosciences, Colorado State University, Fort Collins, CO 80523-1482.
Received April 2004, accepted March 2005.

doi: 10.1111/j.1745-6584.2005.00103.x

hydrogeologic variations (Resistivity: e.g., Kelly 1977; Heigold et al. 1979; Kelly and Frohlich 1985; Ahmed et al. 1988; Cassiani and Medina 1997; Purvance and Andricevic 2000; Yeh et al. 2002; Niwas and de Lima 2003; GPR: e.g., Hubbard et al. 1997; Peretti et al. 1999; Gloaguen et al. 2001; Lesmes et al. 2002), although uncertainties associated with data processing and interpretation do exist.

The ground water research site located on Columbus Air Force Base (CAFB) in Columbus, Mississippi (Figure 1), has a long history of research aimed at understanding ground water flow and contaminant transport in a heterogeneous porous media. There have been two major macrodispersion experiments (MADE-1 and MADE-2; October 1986 through June 1988 and June 1990 to September 1991, respectively) and a Natural Attenuation Study (NATS; August 1995 to September 1997) conducted at the ~30,000-m^2 site (e.g., Boggs and Adams 1992; MacIntyre et al. 1993; Feehley et al. 2000; Julian et al. 2001). One of the major goals of these studies was to test fluid-flow and transport models against flow and transport data collected in a densely instrumented natural system. Each study sampled the ground water using a network of 328 multilevel samplers to monitor the advective-dispersive behavior of injected tracers (bromide and tritium) over time. The spatial and temporal variations of tracer data recorded in such experiments provide excellent benchmarks for flow and transport simulation models.

The spatial variation of hydraulic conductivity obtained from borehole flowmeter tests in >50 wells demonstrated the large degree of heterogeneity at this site as compared to similarly studied sites. For example, the natural log variance of hydraulic conductivity is 4.5 for the MADE site (Rehfeldt et al. 1992) vs. 0.29 for the Borden site located in Canada (Sudicky 1986), 0.26 for the Cape Cod site located in Massachusetts (Hess 1989), or 0.031 for the Twin Lake site located in Minnesota (Moltyaner 1986). These differences in aquifer heterogeneity are attributed to lithology and the aquifer's depositional environment. The CAFB site predominantly comprises a braided fluvial system (BFS) containing a mixture of clay to gravel size sediments, whereas the Borden, Cape Cod, and Twin Lakes sites comprise relatively homogeneous glaciofluvial sediments.

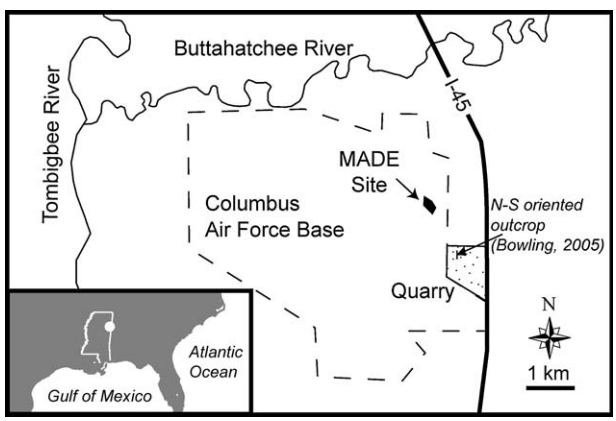

Figure 1. The study area is located on the northeast corner of CAFB (dashed line) and within 1 mile of a sand and gravel quarry examined by Bowling (2005).

In addition to conventional hydrogeological investigation (borehole flowmeter tests, grain-size analyses, and porosity/permeability tests on sediment cores), there have been two previous geophysical studies at the MADE site. The first study was part of the initial characterization of the site that included both surface geophysical methods (direct current [DC] resistivity soundings and profiles, streaming potential and electromagnetics) and borehole geophysical methods (natural gamma, gamma-gamma, neutron, and single-point resistivity) aimed at indirectly measuring the spatial variation of hydraulic conductivity (Boggs et al. 1990). These studies show that surface-derived DC resistivity has a strong relationship with grain size, and borehole resistivity has a general correlation with hydraulic conductivity. Better correlations between borehole resistivity and hydraulic conductivity were limited by disturbance around the wellbore that decreased data quality (Boggs et al. 1990). Boggs et al. (1990) ultimately concluded that the geophysical parameters measured did not have a strong correlation with hydraulic conductivity and therefore relied heavily on direct methods of measurement such as borehole flowmeters. More recently, Tereschuk (1998) applied GPR methods to the MADE site, collecting one north-south two-dimensional (2D) line along the axis of the site and one small (20 $\times$ 20 m) 3D radar cube. Tereschuk (1998) found that GPR was able to resolve the internal stratigraphy of the aquifer and that stratigraphic features imaged were correlatable over distances (1.67 to 5 m) similar to the length of the correlation scale for the hydraulic conductivity distribution (4.8 m; Rehfeldt et al. 1992). This work was an important step in characterizing the MADE site but lacked the spatial coverage to adequately characterize the entire site.

The wide range of clay content and the sensitivity of the clay fraction to depositional controls in aquifer systems, such as that present at the MADE site, result in an excellent environment for the use of geophysical imaging techniques for aquifer characterization. Clay content generally correlates with hydraulic conductivity in clastic aquifers, and variations in clay content strongly affect both electrical resistivity and GPR. As a consequence, clay fraction is both an important hydrogeological parameter and one of the lithological attributes that is best constrained by geophysical studies. This paper presents a geologic model of the MADE site created from the interpretation of two-dimensional DC resistivity and GPR data integrated with previously collected sediment cores, point hydraulic conductivity measurements (Boggs et al. 1990; Boggs and Adams 1992), and a geologic study of an exposed section of the aquifer in a nearby sand and gravel quarry (Bowling 2005). Qualitative comparisons are made between geophysical data, hydrologic data, the new geologic model, and tracer data from the MADE-2 experiment to evaluate the applicability of using geophysical data to better delineate the heterogeneity of fluvial aquifers.

Site Description

The MADE site is located between the Tombigbee and Buttahatchee rivers in the northeastern part of Mississippi (Figure 1) and is composed of Quaternary-aged relict-terraced fluvial deposits (Cook 1998). The majority of the site is located in an open field ~100 by 300 m on the northeast corner of CAFB. Surface topography dips gently to the north at <1 m per 200 m. The high accessibility and relatively flat topography makes this site ideal for geophysical measurements. Bowling (2005) evaluated a suite of geophysical methods, including 50 and 100 MHz GPR, DC resistivity, and seismic reflection, for imaging an exposed sand and gravel quarry wall located 0.75 km to the southeast of the MADE site. Similar lithologic profiles of cores collected at both sites (Figure 2) as well as the close proximity of the sites suggest that quarry interpretations should apply to the MADE site; however, the section examined at the quarry was drained and no hydrological data were available to compare with the geophysical results. Dominant quarry facies are composed of lithologies that vary both horizontally and vertically over ranges of centimeters to meters. The uppermost facies is interpreted as part of the present-day meandering fluvial system (MFS) associated with the Buttahatchee River. This unit extends to depths of 3 m and is characterized by massive sandy clay with several clay-filled channels. A coarser-grained facies composed primarily of channelized gravelly sand with interbedded clay lenses lies between depths of 3 and 9 m and is interpreted as a BFS. Lower-bounding clay-rich sediments serve as an aquitard to the overlying aquifer system. Results presented in Bowling (2005) were used as guidelines for data collection and interpretation at the MADE site.

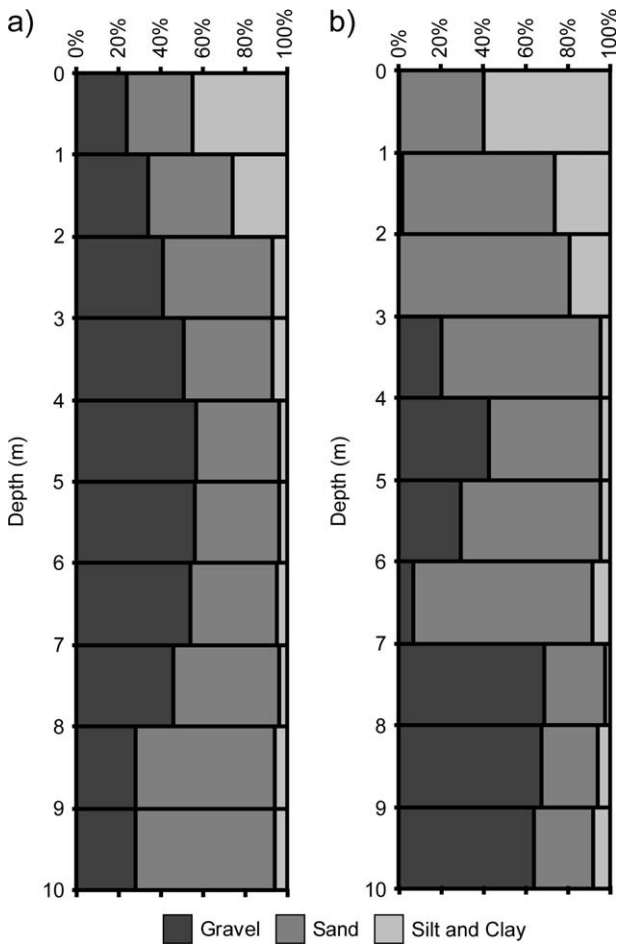

Figure 2. Grain-size analyses for cores from (a) the MADE site and (b) the sand and gravel quarry show similar lithologic profiles. The MADE site profile is a site average based on 214 aquifer samples from >20 cores (Boggs and Adams 1992). The sand and gravel quarry profile is from one core; therefore, there will be some minor differences in the sand-gravel percentage. However, note the similarity between silt and clay fractions and the variation in sand and gravel between the two sites. The variation of sand and gravel is due to the extremely heterogeneous nature of the braided fluvial section.

Generally, the aquifer is referred to as all sediments above the lower-bounding clay-rich unit. The depth to the base of the aquifer averages 11 m but varies between 10 and 16 m (Boggs et al. 1990). Based on depth-averaged hydraulic conductivity data (Boggs et al. 1990), the site can be divided into zones of lower conductivity at the south and north ends, and a zone of higher conductivity near the center of the site (Figure 3). The correspondence of the higher-conductivity zone with the location of a meander scar visible in historic aerial photographs (Rehfeldt et al. 1992) has led some (e.g., Julian et al. 2001) to believe these zones are related. If so, the channel would extend to depths of 5 to 7 m and have a strong influence on subsurface fluid flow. Based on an analysis of hydraulic conductivity data and sedimentological data, Rehfeldt et al. (1992) concluded that there was subsurface evidence for the existence of a paleochannel beneath the meander scar, although its edges and depth were poorly defined. This interpretation was supported by Sturm (2000) on the basis of a preliminary interpretation of GPR and core data collected at the site, although Sturm argued that the trend of the subsurface channel was perpendicular to the surface meander scar.

Methodology

The geophysical data set used in this study consists of 36 GPR survey lines and 13 resistivity lines (Figure 4). GPR data were collected in 1999 shortly after the NATS while the site was still populated with >300 multilevel sampling wells (Sturm 2000). The presence of the wells complicated GPR survey geometry such that lines varied in separation distance but were on average 12 m apart. Other than resulting in slightly irregular line spacing, the wells had only a minor effect on data quality because the well casing was polyvinyl chloride. The GPR data grid (Figure 4a) was surveyed and marked with plastic surveyor's flags at each line intersection. GPR data were collected using 50-MHz bistatic antennas attached at 2-m separation to a plywood sheet that was dragged along the survey lines. Traces were collected continuously while moving the antennas at a constant speed, resulting in an average trace spacing of 8 cm. Location information was recorded by manually triggering a timing mark in each recording file when the antenna sled passed each survey flag. Traces had a length of 512 ns with

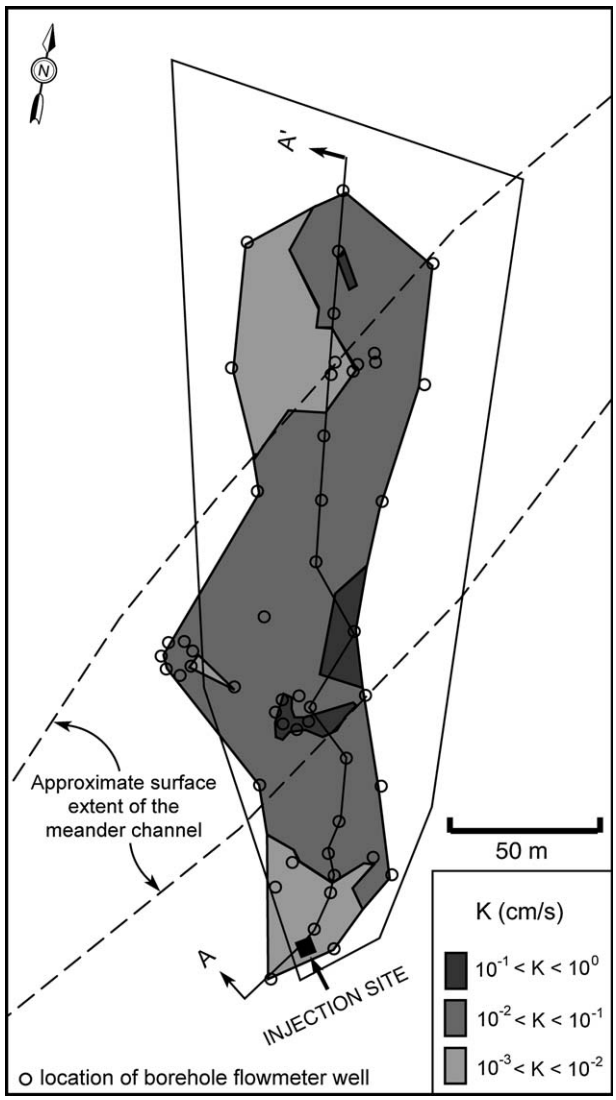

Figure 3. Depth-averaged hydraulic conductivity measured by borehole flowmeters (modified from Boggs et al. 1990; Rehfeldt et al. 1992). General flow direction is from the south to the north. Note: Cross section A-A′ can be found in Figure 14.

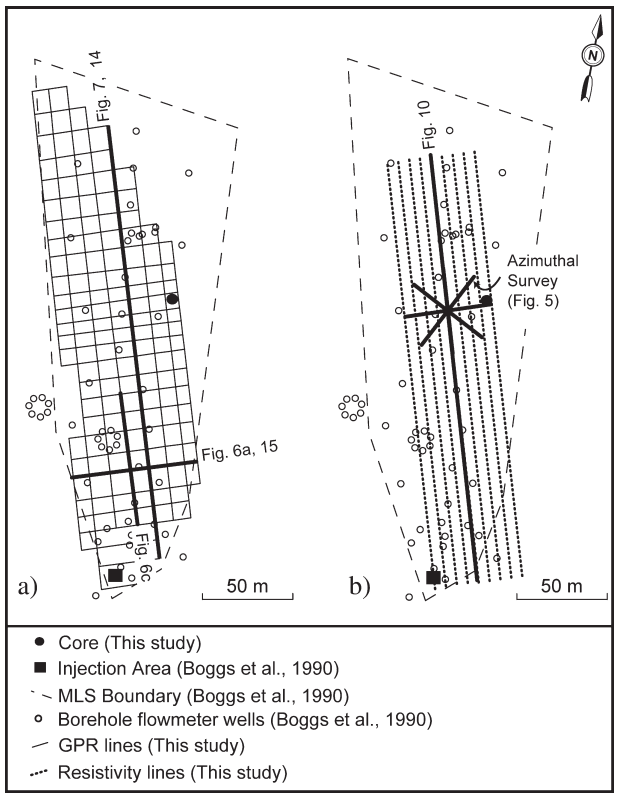

Figure 4. Geophysical surveys were collected in relation to previous work performed at the MADE site. The boundary (dashed line) of multilevel sampling wells and the locations where hydraulic conductivity measurements (open circles) were taken (Boggs et al. 1990) are shown for reference. (a) GPR surveys consisted of 36 lines of 2D data. (b) DC resistivity surveys were collected predominantly along the axis of the site as well as an azimuthal survey near 150 m north.

a 1.6-ns sample interval and were vertically stacked 4 times. Data processing consisted of a band-pass filter with corner frequencies of 10, 20, 40, and 60 MHz to remove high-frequency noise and trace gain using an automatic gain control (AGC) function with a 16-ns AGC window. Data processed with AGC do not preserve relative amplitude information but enable interpretation of reflectors down to the maximum recorded depth of 14.7 m. Because the survey area is essentially flat, a static time shift was applied to each trace so that all surface reflections were at time zero. This static correction was necessary because the antenna sled was occasionally lifted off the ground to avoid obstacles. Data were converted to SEG-Y format and imported into the Seismic Micro-Technology Inc. Kingdom Suite software for interpretation (www.seismicmicro.com). Data were interpreted in two-way travel time and resulting horizons converted to depth using a constant two-way radar velocity of 0.067 m/ns. The radar wave velocity was determined from common midpoint surveys at this site (Tereschuk 1998) and at the nearby quarry (Bowling 2005) using hyperbolic moveout semblance analysis (Yilmaz 1987). Although there may be some error involved with using a constant radar wave velocity for time-depth conversion, the velocity used was verified by comparing the depth of the aquifer base, as interpreted from GPR, to well data published in Boggs et al. (1990).

Two-dimensional DC surface resistivity data were collected with an IRIS Instruments Syscal Pro 48 electrode automatic surveying system in a manner similar to that discussed by Dahlin (2001). Survey lines (9 lines, 235 m in length) were oriented parallel to the long axis of the site (Figure 4b). Lines were spaced 6 m apart to approximately coincide with the location of selected GPR lines and yet maintain constant line spacing. A dipole-dipole configuration with 5-m electrode spacing was used, resulting in 1111 data points per survey line. After editing spurious measurements (attributed to poor electrode-ground coupling and proximity of some electrodes to wells), the resistivity data were inverted using the Geotomo RES2DINV software (Loke 2002), which is based on the least squares algorithm of Sasaki (1992). Root mean square differences between measured and calculated resistivity pseudosections are typically <5%.

Collection of 2D resistivity data involves simpler array design and postprocessing than 3D data. However, in many areas anisotropic resistivity fabrics necessitate the use of a 3D survey (Dahlin and Bernstone 1997). In order to investigate macroscopic subsurface anisotropy (directional variations in resistivity at scales >0.25 m), a separate azimuthal survey was conducted at the center of the site. The azimuthal survey showed no substantial directional variation in subsurface resistivity at this spatial scale (Figure 5). Therefore, a quasi-3D image of the subsurface resistivity structure of the site was obtained by simultaneous inversion of all nine longitudinal resistivity lines using the Geotomo software RES3DINV (http://www.geoelectrical.com). The program is based on the least squares algorithm of Li and Oldenburg (1992) and implements smoothness constraints on the resistivity solution described by deGroot-Hedlin and Constable (1990) and Sasaki (1992). In general, resistivity inversion provides a nonunique result. However, the smoothness constraints, although reducing resolution, greatly limit the range of acceptable solutions. In this research, we adopted identical vertical and horizontal smoothing constraints using the parameters described by Loke (2002). Additionally, the inversion was weakly constrained to provide a solution as close as possible to the average uniform 600-ohm-m half space used as a starting model (Li and Oldenburg 1992). Inversion results of a survey conducted at the nearby gravel quarry obtained with the software used here and the DCIP software from the University of British Columbia (http://www.geop.ubc.ca/ubcgif; based on the algorithm of Li and Oldenburg 2000) yielded similar results, with estimated resistivity values in the subsurface generally agreeing to within <10%.

Both 2D and 3D resistivity inversions were performed on the data. 2D resistivity inversions used a finer grid (0.5 × 0.5 m) than the 3D resistivity inversion, which contained >9000 measurements and necessarily used a coarser model grid (1.75 m vertical × 5 m horizontal). Both inversions show similar trends in resistivity. The 3D inversion is better at showing overall trends, while 2D inversions are used for assessing thickness of individual layers. Model results were validated by comparison with core data from the MADE site (Boggs et al. 1990) and to exposure at the nearby sand and gravel quarry (Bowling 2005).

Results and Interpretation

Based on reflection character and DC resistivity variations, four main facies are recognized. The upper two facies correspond to the MFS and underlying BFS described by Bowling (2005) in the nearby quarry outcrop. The third unit consists of sand, described as "fine-grained, frequently containing thin interbedded clay and silt laminations" (Boggs et al. 1990), which differs from the gravelly-sand matrix that composes the braided system. This unit is referred to as "fine-grained sand" here, although there may be a significant clay and silt component. The fourth facies corresponds to a clay-rich unit that underlies the entire site and serves as an aquitard (Boggs et al. 1990).

Ground Penetrating Radar

Four different scales of radar facies are recognized in the area, first order being the largest scale and fourth order being the smallest scale. First-order reflection boundaries mark the bases of the MFS, BFS, and fine-grained sands and can be correlated through the entire site (Figure 6). Second-order boundaries are recognized between first-order boundaries and can also be correlated throughout the entire site. In the BFS, second-order boundaries truncate smaller-scale third-order boundaries, thereby indicating periods of regional fluvial erosion, while in the MFS, second-order boundaries are interpreted as floodplain diastems. Third-order reflection boundaries, represented by discontinuous intrafacies

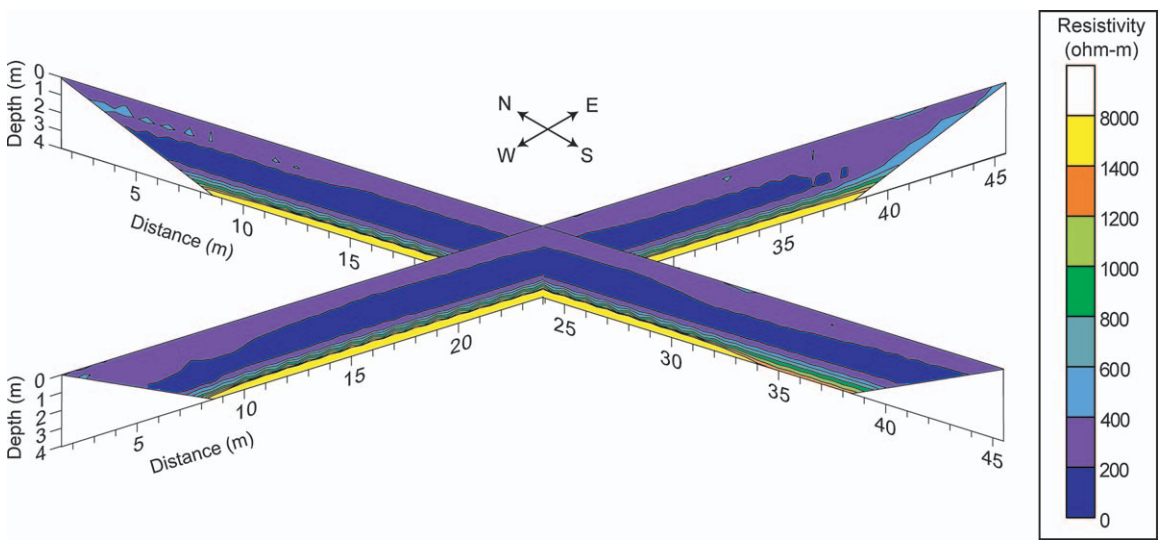

Figure 5. An azimuthal resistivity survey was collected that demonstrates no directional resistivity variations exist at the site. See Figure 4 for location.

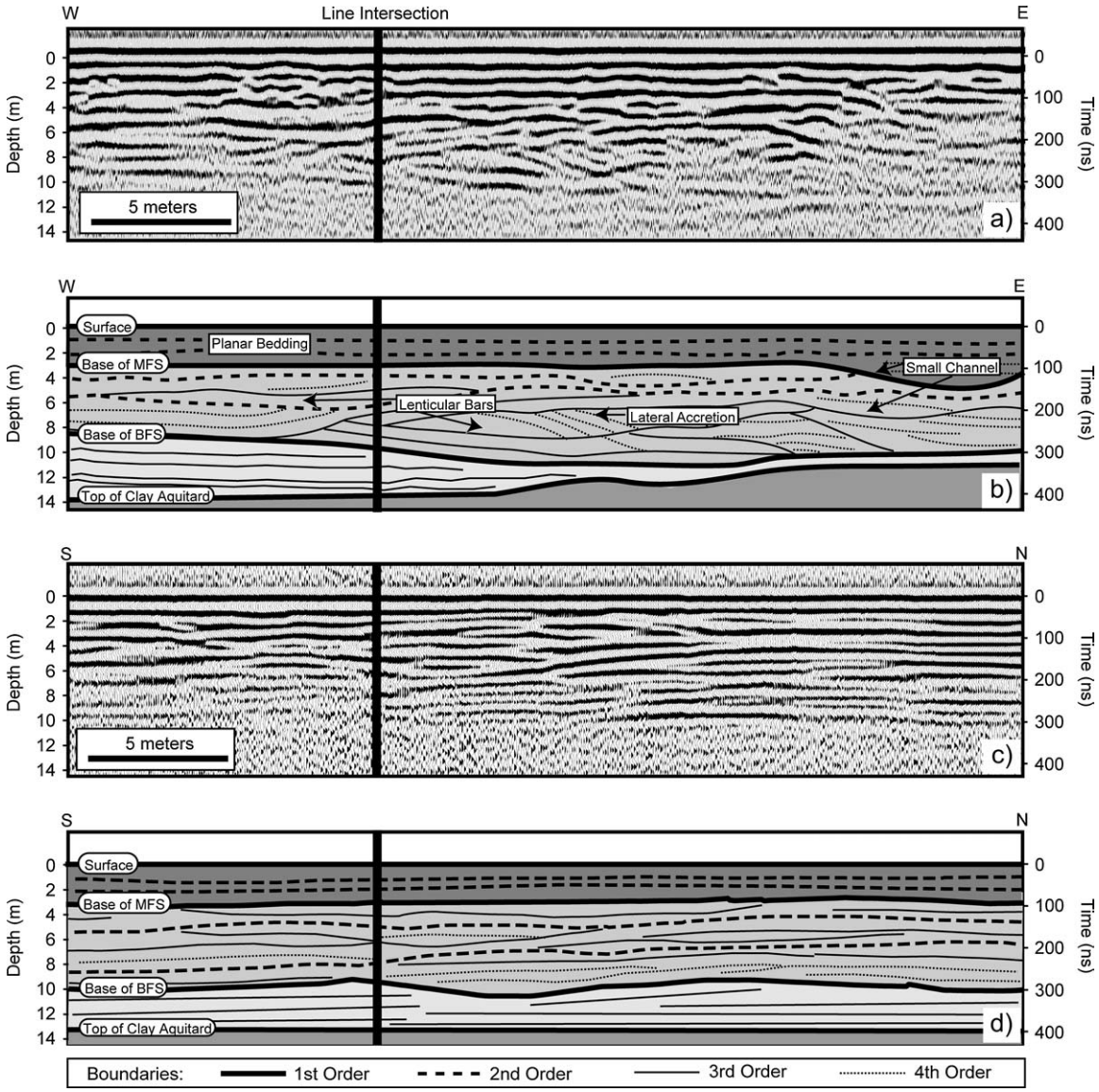

Figure 6. Four different scales of radar facies were recognized in the area, first order being the largest scale (correlatable throughout the study area) and fourth order being the smallest scale (<10 m in extent). (a) East-west and (c) north-south oriented GPR lines that show characteristic radar facies and (b, d) line drawing interpretations. The heavy vertical line indicates the intersection of the two profiles. See Figure 4 for location.

reflections, are correlated between second-order surfaces. Third-order boundaries define small channels (5 to 10 m wide) and interchannel bars, most of which are lenticular in shape. Fourth-order reflection boundaries are the smallest-scale recognizable units that range in length from 1 to 5 m and are bound by third-order surfaces. Inclined and horizontal parallel reflectors within lenticular bars and channels are identified as fourth-order boundaries representing accretion. Due to the relatively large grid spacing (~12 m) in relation to the small size of third- and fourth-order reflection boundaries, these could not be correlated throughout the site.

Structure maps of the first- and second-order surfaces (Figures 7a through 7g) show the depth associated with each layer and the morphological variations between each depositional system. The meandering fluvial facies is 2 to 4 m thick (Figure 8a), consisting of subhorizontal, laterally continuous reflectors (Figures 7b to 7d). A major channel structure within this unit is located in the middle of the MADE site (Figure 7c). The channel was estimated to be 2 m deep and 150 m wide. Three horizontal layers can be mapped both north and south of the channel in what is interpreted as floodplain. Interpretation of additional structures within the meandering system, such as innerchannel stratification, is beyond the resolution of the GPR data. The base of the MFS was mapped throughout the area as a nearly planar southeast dipping surface (Figure 7d).

The lower braided fluvial facies is 5 to 10 m thick (Figure 8b), consisting of bidirectional dipping discontinuous reflectors that form third- and fourth-order stratigraphic boundaries between second-order boundaries (Figures 7e and 7f). The base of the BFS was mapped as an irregular northwestward dipping surface throughout

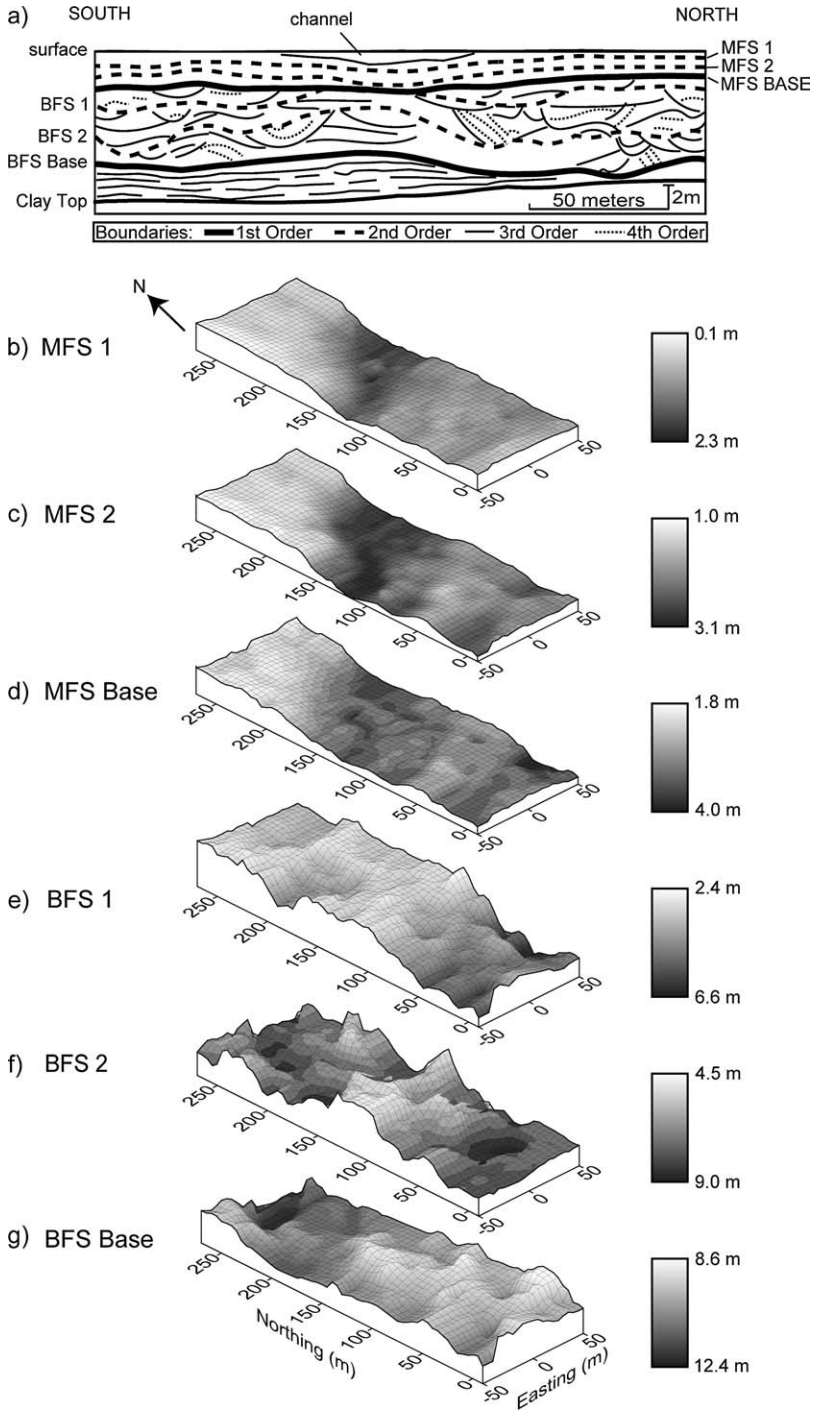

Figure 7. (a) A radar stratigraphy line drawing for a longitudinal GPR line (see Figure 4 for location). (b-g) Surface contour maps of GPR facies boundaries arranged in order of increasing depth and interpolated by kriging. First- and second-order facies boundaries were correlatable across the entire site. First-order boundaries mapped include the bases of (d) the MFS and (g) BFS. Second-order intra-section boundaries mapped are (b) MFS-1, (c) MFS-2, (e) BFS-1, and (f) BFS-2. MFS-1 and MFS-2 are interpreted as floodplain diastems, while BFS-1 and BFS-2 are interpreted as erosional surfaces.

the site based on a continuous subhorizontal reflector below braided fluvial facies (Figure 7g). This interpreted surface shows less relief than the second-order interval surfaces. However, the structure maps of the first- and second-order BFS boundaries show more irregular topography than first- and second-order MFS boundaries. Relief on BFS boundaries varies from 4 to 5 m as opposed to 1- to 2-m relief for the MFS boundaries.

In places, the base of the BFS mapped in this study is up to 5 m shallower than the interpretation of aquifer thickness by Boggs et al. (1990). The interval between the two is interpreted to represent the fine-grained sands. This unit is bound both above and below by strong, nearly continuous reflections. Radar stratigraphy of the fine-grained sands consists of low signal-to-noise ratio, discontinuous, subhorizontal planar reflectors that are

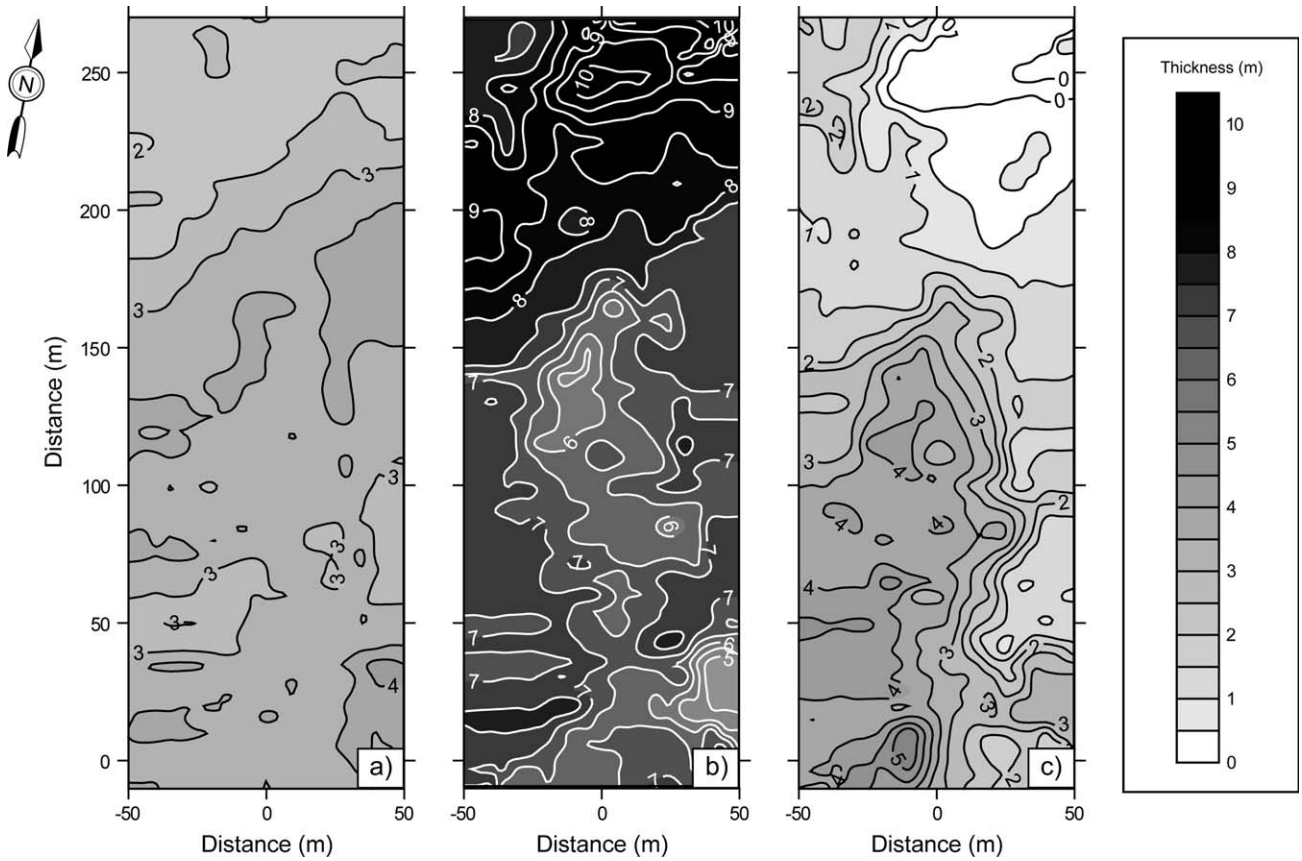

Figure 8. Isopach maps of (a) the MFS, (b) the BFS, and (c) the fine-grained sands that underlie the BFS based on GPR data.

distinct from the overlying BFS (Figures 6a and 6b). These fine-grained sands make up the lower part of the aquifer and have a maximum thickness of 5 m to the south but thin and pinch out to the north (Figure 8c).

Depth to the top of the clay aquitard (range 10 to 16 m), recognized in cores by Boggs et al. (1990), correlates to a continuous reflector at the base of the GPR data. This reflector was not correlated across the entire site because the GPR data reached a maximum of 15 m; however, in areas where it was imaged, the GPR data and the map by Boggs et al. (1990) agree.

DC Resistivity

Resistivity data were interpreted to infer a quasi-3D model using the 2D inversion of dipole-dipole data from parallel profiles. The model shows four main units (Figure 9). The upper unit is a thin, low-resistivity (200 to 700 ohm-m) layer ranging from 2 to 4 m in thickness that correlates with the MFS as mapped with the GPR data set. This layer also contains two linear zones oriented approximately east-west across the site, one with high resistivity compared to surrounding areas and the other with relatively low resistivity. The northern zone is a low-resistivity (<100 ohm-m) feature ~50 to 60 m wide. The southern zone (~75 m north) is highly resistive (>4000 ohm-m) and is ~10 m wide. The southern zone is an area of disturbed ground, which is the result of utility line emplacement just prior to surveying. This utility trench postdates the GPR survey and was backfilled with loosely compacted sand and gravel. The disturbed ground filling the utility trench resulted in an area of anomalously high resistivity. The utility line itself does not appear on the resistivity image, indicating that it had little effect on current flow and did not produce a measurable electrical potential during the survey. This inference is supported by self-potential measurements between adjacent electrode pairs that were collected during the survey as a quality control measure; background electrical potential gradients in the vicinity of the trench were comparable to those measured elsewhere in the survey area, indicating it did not bias the resistivity signal measured. The lack of an effect of the utility line is most likely due to the facts that the utility line is insulated cable and was not yet in use at the time of the survey. The wider, low-resistivity northern feature (Figure 9a) has resistivities similar to areas of high clay content mapped at the nearby quarry outcrop (Bowling 2005). This feature corresponds to the location of the paleochannel visible in historical aerial photographs (Figure 3) and mapped with the GPR data set (Figure 7). Low resistivity variations beneath the surface expression of the paleochannel are confined to the upper 1.75 m in the quasi-3D model derived from simultaneous inversion of the resistivity lines but are ~1.25 m deeper in the 2D models (Figure 10). A portion of the azimuthal survey performed in the vicinity of the channel was coincident with one of the longitudinal lines (Figure 10). This azimuthal line imaged shallower depths at much higher resolution than the axial line due to the smaller electrode spacing (1 m). The base of the

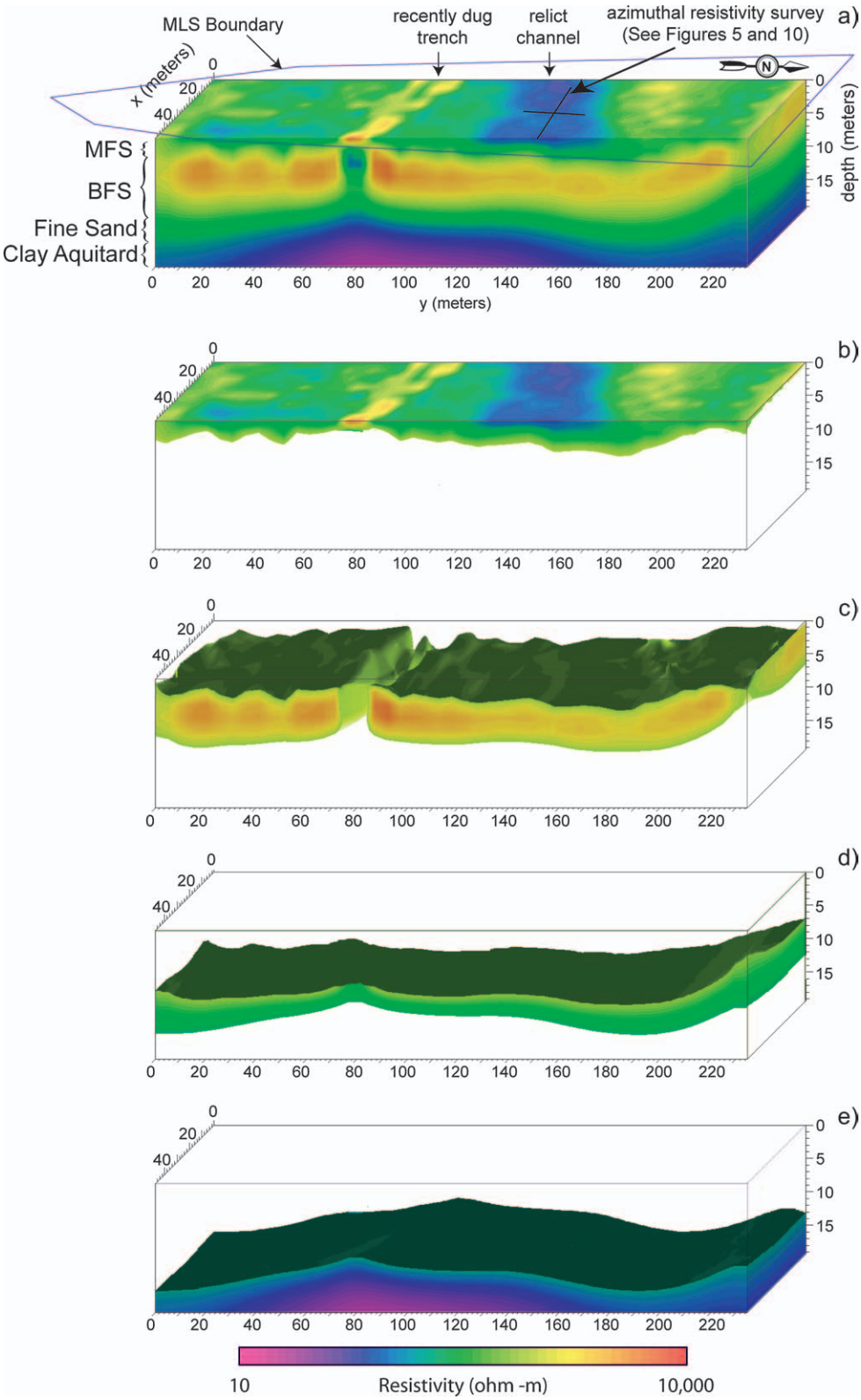

Figure 9. Results of the 3D resistivity inversion. The block diagram (a) of the inversion volume shows a recently disturbed area, a relict channel with clay fill, and three layers. The three layers are subdivided into (b) moderate resistivities associated with sandy-clay facies of the MFS, (c) high resistivities associated with gravelly sands of the BFS, (d) moderate resistivities associated with fine-grained sands just below the BFS, and (e) low resistivities associated with the high clay content of the underlying aquitard.

low-resistivity layer (i.e., the base of the channel) is interpreted from the higher-resolution azimuthal resistivity data to be at 3-m depth, which corresponds to the depth of the channel interpreted on the GPR data.

Resistivity surveys conducted by Boggs et al. (1990) mapped horizontal resistivity variations (100 to 4000 ohm-m) at a depth corresponding to the upper resistivity layer interpreted here but over a much larger area and

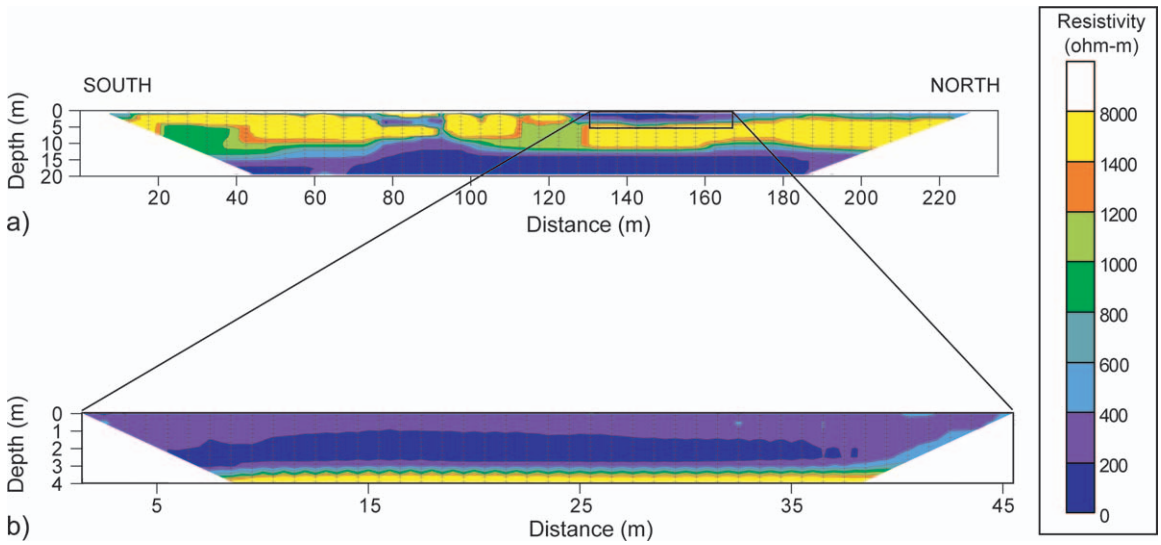

Figure 10. Two DC resistivity surveys were taken perpendicular to the paleochannel. (a) Lower-resolution regional survey of the area. (b) High-resolution survey located over the channel. Channel depths in (b) are interpreted to be ~3 m.

coarser measurement spacing (30.5 m). Although not interpreted as such, the study by Boggs et al. (1990) shows two linear regions of relatively low resistivity in the area (Figure 11). The first crosses the MADE site, and the second lies just to the south. These two zones of low resistivity, which extend to depths of <3 m, correspond with arms of the meander scar visible in aerial photographs. The northern zone also correlates with the location of low resistivity in profiles from this study.

The second layer in the resistivity models obtained here has higher resistivities (1000 to 4000 ohm-m) than the near surface, averages 8 to 10 m in thickness, and correlates well with the depth of the BFS as mapped with the GPR data set. The water table was either not resolved or is at the same depth as the top of the second resistivity layer. The latter interpretation is consistent with average annual water table depths measured in wells in the study area, which typically show a water table close to the top of the BFS. The third resistivity layer extends from 12- to 15-m depth, has a relatively low resistivity (100 to 200 ohm-m), and correlates with the fine-grained sands. Low resistivities (<100 ohm-m) associated with the clay

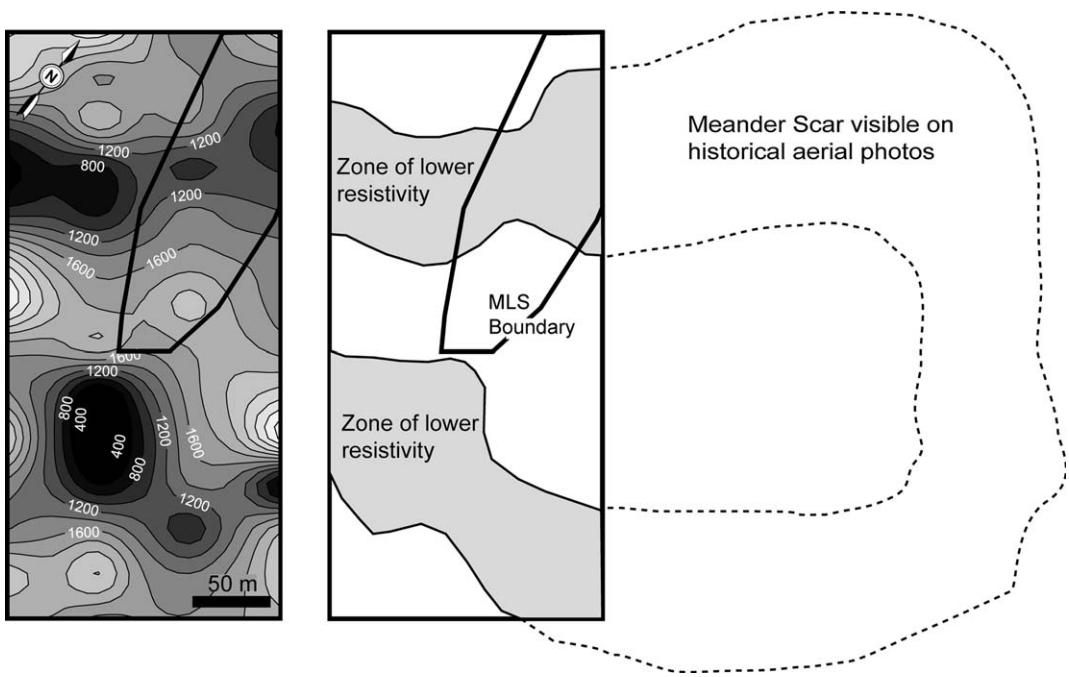

Figure 11. Reinterpretation of a coarse-grid, regional resistivity survey (map is average resistivity approximately from the surface to 1 to 2 m depth) after Boggs et al. 1990. In this area, lower resistivities indicate a higher clay fraction, which conform to locations of the channel fill that crosses the MADE site (multilevel sampler boundary). A second zone of lower resistivities to the south could be related to another extension of the abandoned channel.

aquitard extend to the base of the model, forming the fourth layer of the resistivity model and aquitard to the overlying sediments.

Bowling (2005) gives an empirical relationship between resistivity and percent silt and clay in the area based on a survey of the nearby quarry outcrop. Using their relationship and the resistivity layers defined previously, the upper resistive layer (~0- to 4-m depth; 200 to 700 ohm-m) would contain between 40% and 60% silt and clay, the middle, highly resistive layer (~4- to 12-m depth) would contain <30% silt and clay with resistivities above 1800 ohm-m containing virtually no silt and clay, and the lower layer (~12-to 14-m depth; 200 to 100 ohm-m) would be >60% clay by weight. Recognizing that there is some depth error (~1 m) associated with the layer contacts as derived from the resistivity model, these findings generally correspond with the core taken at the MADE site (which penetrated the upper two layers) as well as GPR facies (Figure 12).

Discussion

DC resistivity data acquired at the MADE site is in general agreement with the first-order facies boundaries identified in the GPR data; the bases of the MFS and BFS and top of the clay-rich unit are detected at similar depths with both methods. These first-order boundaries correspond to changes in depositional environments, thereby affecting lithology and stratigraphy. The only second-order boundary imaged by both techniques is the paleochannel in the MFS, which is likely to be finer grained than the surrounding sediments. The channel position is coincident in both geophysical datasets; however, the channel mapped using GPR data is wider (~120 m) than that estimated from the resistivity data (~70 m). Differences between DC resistivity and GPR interpretations are attributed to the different physical properties measured and resolutions of each technique. GPR data had high vertical and horizontal resolution (on the order of decimeters). However, the low reflector amplitude at the depth the data were gained, resulted in loss of relative amplitude and consequently lithological information. Conversely, resistivity data possess relatively low vertical and horizontal resolution (on the order of meters) but are sensitive to lithological information such as relative clay percentage. GPR data also image stratigraphic variation to a higher degree, while the DC resistivity collected here tends to blur those boundaries. An example of the correlative nature of radar facies to depositional environments is shown by comparison of a sediment core taken at the site to the GPR facies (Figure 12).

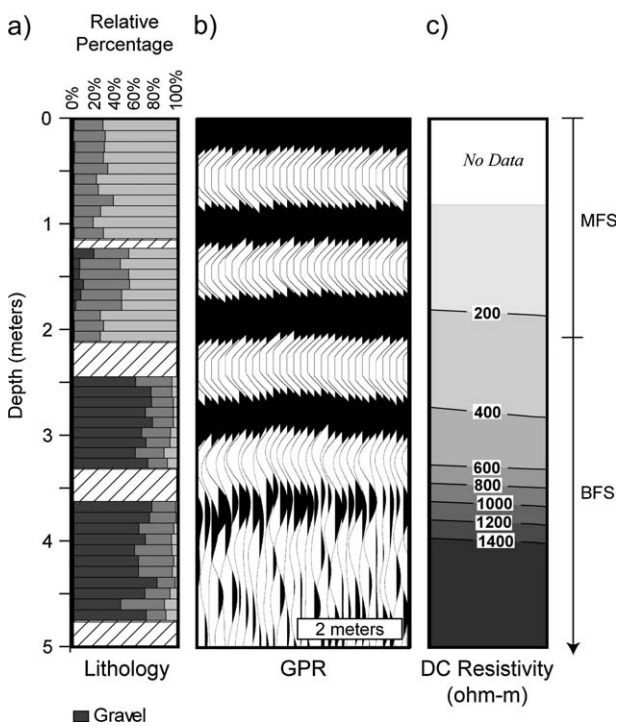

Figure 12. Changes in lithology visible in (a) core collected at the MADE site correlate with (b) GPR reflections and (c) resistivity taken from lines crossing the core location.

The four-layer geological interpretation of the MADE site in Figure 13 (MFS [0 to 4 m], BFS [4 to 12 m], fine-grained sands [12 to 14 m], and a clay-rich aquitard [>14 m]) agrees with the variations in hydraulic conductivity measured by conventional hydrological methods (Figure 14). The water table at the MADE site varies seasonally between 1 and 3 m below the land surface (Boggs et al. 1990). This suggests that the middle facies (the BFS) contains the main aquifer that serves as the conduit for contaminants transported during each of the large-scale tracer tests. The paleochannel, recognized by previous researchers on the basis of aerial photographs and mapped here using DC resistivity and GPR data, is confined to the upper facies (the MFS) and does not extend into the braided system (i.e., the water table aquifer). The paleochannel does not overlap with even the shallowest of hydraulic conductivity measurements made below the water table from Boggs et al. (1990) and therefore should not have a major effect on subsurface flow and contaminant transport (Figure 14). A majority of the aquifer section measured by borehole flowmeters lies within the BFS. The large values of hydraulic conductivity can be attributed to the coarse sediments typically carried by braided streams. The dynamic nature of braided streams involves multiple channels with multiple episodes of erosion and deposition that can account for the large variations in K-values. The low-conductivity section ($K < 10^{-4}$ cm/s) that lies below the base of the BFS mapped here correlates with the fine-grained sands (Figures 13 and 14).

Plume data from the MADE-2 tritium tracer experiment (Boggs et al. 1993) were interpolated using a linear distance algorithm in three dimensions. The injected tritium solution moved downgradient from the injection point at small concentrations (Feehley et al. 2000). After 328 d, a majority of the tracer remained within 50 m of the injection site with a low concentration plume (<10 pCi) extending for 200 m. The plume was confined to the BFS, indicating that first-order GPR boundaries define flow pathways (Figure 15). Plume shape and the locations of high tracer concentrations appear to be influenced by GPR second- and third-order boundaries (Figure 15). Note that tracer concentrations >10 pCi spread out at the base of the BFS unit and do not penetrate significantly

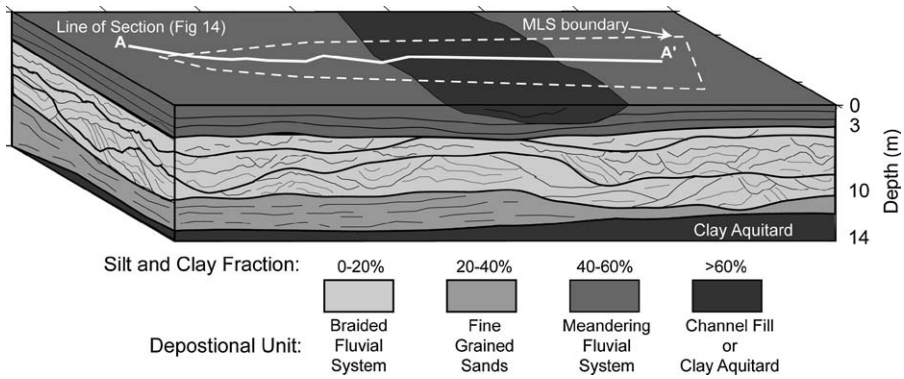

Figure 13. Geologic model of the MADE site. Interpretation of 2D geophysical surveys indicates three facies of different depositional origin; an MFS, a BFS, and underlying fine-grained sands and a clay-rich aquitard. Clay fractions are estimated from the resistivity surveys and a relationship by Bowling (2005).

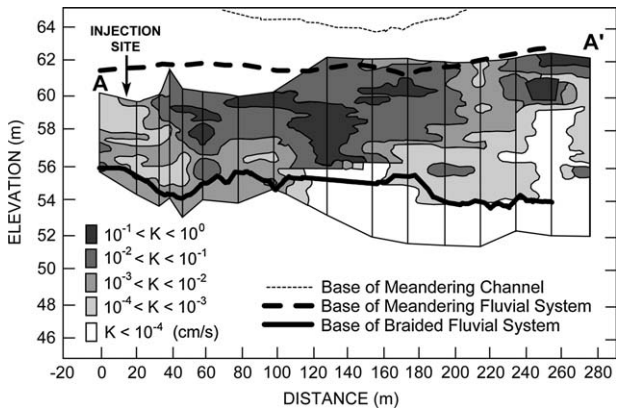

Figure 14. Bases of the MFS and BFS interpreted on a GPR line (Figure 4a) subparallel to and overlain on a hydraulic conductivity (*K*) cross section (Figure 3) from Boggs et al. (1990). The stratigraphic horizons correlate well with the top and bottom of the aquifer as defined by hydraulic conductivities $>10^{-3}$ measured by borehole flowmeters. The channel interpreted in GPR data shows up as a shallow horizon and is not measured by borehole flowmeters. Low conductivities below the BFS correlate to the finer-grained sands and clay that form the underlying aquitard.

into the underlying finer-grained sands. Based on this, the unconfined aquifer hydrologically consists entirely of the BFS unit.

Conclusions

A hydrogeological conceptual model of the MADE site (Figure 13) is constructed from interpretations of newly collected DC resistivity and GPR measurements of the MADE site that were integrated with previously collected borehole flowmeter measurements and sediment cores. Based on these data, the MADE site consists of a stratigraphically and hydrologically complex sandy-gravel aquifer deposited by a BFS at depths of ~4 to 12 m. Shallower depths correspond to a laterally homogenous layer of predominately silt and clay, with smaller amounts of sand and gravel most likely deposited by a MFS. A channel within the MFS is probably silt and/or clay filled based on low resistivities but is too shallow to influence ground water flow except for effects on aquifer recharge. In conjunction with previously collected *K*-data, resistivity data indicates that the BFS unit should contain the highest hydraulic conductivity and that the MFS and fine-grained sands of facies 3 should have lower conductivities. The GPR data indicates that the BFS is more heterogeneous than the MFS and the fine-grained sands, based on its more complex depositional history. Although the fine-grained sand unit is part of the aquifer (Boggs et al. 1990), comparison of plume tracer data from the MADE-2 experiment suggests that this unit did not participate in tracer transport. Overall, contaminant transport appears to be confined principally to the interval of

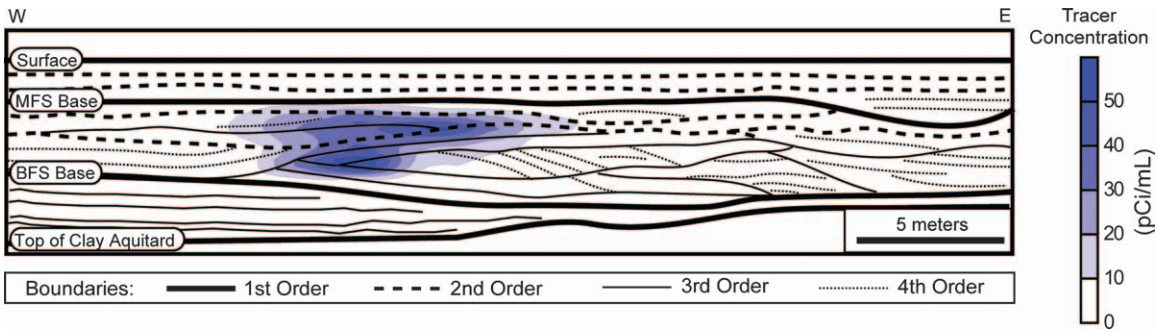

Figure 15. Migration of tritium injected during the MADE-2 tracer experiment exhibits a correlation with first-, and to a lesser degree second- and third-, order radar stratigraphic boundaries. See Figure 4a for locations of injection point and GPR transect.

sediments deposited by a BFS, and within this unit, flow partitioning is controlled by allostratigraphic units (strata between second-order surfaces), and small-scale channel and/or bar depositional variations (strata between third- and fourth-order surfaces).

Acknowledgments

We thank Jerry McJunkin of Terraplus Inc. for providing a scholarship to J.C.B. that enabled us to conduct the resistivity research. Great thanks go to the many students and colleagues who aided in collecting the seismic part of this experiment. BP-Amoco and the University of Alabama Department of Geological Sciences provided Summer Research Fellowships to J.C.B. We thank Jack Hermance, Ken Rehfeldt, and David Hyndman for valuable constructive criticism that improved the manuscript. We also thank Troy Stewart for aid in gaining access to the MADE site. This research was partially funded by NSF Grants EAR-0216520 and EAR-0003511.

References

Ahmed, S., G.D. Marsily, and A. Talbot. 1988. Combined use of hydraulic and electrical properties of an aquifer in a geostatistical estimation of transmissivity. *Ground Water* 26, no. 1: 78–86.

Boggs, J.M., and E.E. Adams. 1992. Field study of dispersion in a heterogeneous aquifer. 4: Investigation of absorption and sampling bias. *Water Resources Research* 28, no. 12: 3325–3336.

Boggs, J.M., L.M. Beard, S.E. Long, M.P. McGee, W.G. MacIntyre, C.P. Antworth, and T.B. Stauffer. 1993. Database for the second macrodispersion experiment (MADE-2). EPRI TR-102072. Research Project 2485-5. Norris, Tennessee: TVA Engineering Laboratory.

Boggs, J.M., S.C. Young, D.J. Benton, and Y.C. Chung. 1990. Hydrogeologic characterization of the MADE site. EPRI EN-6915. Research Project 2485-5. Norris, Tennessee: TVA Engineering Laboratory.

Bowling, J.C. 2005. Integrated geophysical and geological investigation of a heterogeneous fluvial aquifer in Columbus, Mississippi. Ph.D. diss., Department of Geological Sciences, University of Alabama.

Cassiani, G., and M.A. Medina Jr. 1997. Incorporating auxiliary geophysical data into ground-water flow parameter estimation. *Ground Water* 35, no. 1: 79–91.

Cook, J.C. 1998. Geomorphology of the youngest terrace of the Tombigbee River north of Columbus, Mississippi. M.S. thesis, Department of Geosciences, Mississippi State University.

Dahlin, T. 2001. The development of DC resistivity imaging techniques. *Computers & Geosciences* 27, 1019–1029.

Dahlin, T., and C. Bernstone. 1997. A roll-along technique for 3D resistivity data acquisition with multi-electrode arrays. In *Proceedings of the Symposium on the Application of Geophysics to Environmental and Engineering Problems*, 927–935. Reno, Nevada: Environmental and Engineering Geophysical Society.

deGroot-Hedlin, C., and S. Constable. 1990. Occam's inversion to generate smooth, two-dimensional models from magnetotelluric data. *Geophysics* 55, no. 12: 1613–1624.

Feehley, C.E., C. Zheng, and F.J. Moltz. 2000. A dual-domain mass transfer approach for modeling solute transport in heterogeneous aquifers: Application to the macrodispersion experiment (MADE) site. *Water Resources Research* 36, no. 9: 2501–2515.

Frohlich, R.K., J.J. Fisher, and E. Summerly. 1996. Electric-hydraulic conduction correlation in fractured crystalline bedrock: Central Landfill, Rhode Island, USA. *Journal of Applied Geophysics* 35, no. 4: 249–259.

Gloaguen, E., M. Chouteau, D. Marcotte, and R. Chapuis. 2001. Estimation of hydraulic conductivity of an unconfined aquifer using cokriging of GPR and hydrostratigraphic data. *Journal of Applied Geophysics* 47, 135–152.

Heigold, P.C., R.H. Gilkeson, K. Cartwright, and P.C. Reed. 1979. Aquifer transmissivity from surficial electrical methods. *Ground Water* 17, no. 4: 338–345.

Hess, K.M. 1989. Use of borehole flowmeter to determine spatial heterogeneity of hydraulic conductivity and macrodispersivity in a sand and gravel aquifer, Cape Cod, Massachusetts. Paper presented at NWWA Conference on New Field Techniques for Quantifying the Physical and Chemical Properties of Heterogeneous Aquifers, Houston, Texas.

Hubbard, S.S., Y. Rubin, and E. Majer. 1997. Ground-penetrating-radar-assisted saturation and permeability estimation in bimodal systems. *Water Resources Research* 33, no. 5: 971–990.

Julian, H.E., J.M. Boggs, C. Zheng, and C.E. Feehley. 2001. Numerical simulation of a natural gradient tracer experiment for the natural attenuation study: Flow and physical transport. *Ground Water* 39, no. 4: 534–545.

Kelly, W.E. 1977. Geoelectric sounding for estimating aquifer hydraulic conductivity. *Ground Water* 15, no. 6: 420–425.

Kelly, W.E., and R.K. Frohlich. 1985. Relations between aquifer electrical and hydraulic properties. *Ground Water* 23, no. 2: 182–189.

Kosinski, W.K., and W.E. Kelly. 1981. Geoelectric soundings for predicting aquifer properties. *Ground Water* 19, no. 2: 163–181.

Lesmes, D.P., S.M. Decker, and D.C. Roy. 2002. A multiscale radar-stratigraphic analysis of fluvial aquifer heterogeneity. *Geophysics* 67, no. 5: 1452–1464.

Li, Y., and D.W. Oldenburg. 2000. 3-D Inversion of induced polarization data. *Geophysics* 65, no. 6: 1931–1945.

Li, Y., and D.W. Oldenburg. 1992. Approximate inverse mappings in DC resistivity problems. *Geophysical Journal International* 109, no. 2: 343–362.

Loke, M.H. 2002. *Tutorial: 2-D and 3-D Electrical Imaging Surveys*. www.geoelectrical.com. Accessed May 2004.

MacIntyre, W.G., J.M. Boggs, C.P. Antworth, and T.B. Stauffer. 1993. Degradation kinetics of aromatic organic solutes introduced into a heterogeneous aquifer. *Water Resources Research* 29, no. 12: 4045–4052.

Moltyaner, G.L. 1986. Stochastic versus deterministic: A case study. *Hydrogeologie* 2, 183–196.

Niwas, S., and O.A.L. de Lima. 2003. Aquifer parameter estimation from surface resistivity data. *Ground Water* 41, no. 1: 94–99.

Peretti, W.R., M.D. Knoll, W.P. Clement, and W. Barrash. 1999. 3-D GPR imaging of complex fluvial stratigraphy at the Boise hydrogeophysical research site. In *Proceedings of the Symposium on the Application of Geophysics to Environmental and Engineering Problems*, 555–564. Oakland, California: Environmental and Engineering Geophysical Society.

Ponzini, Y., A. Ostroman, and M. Molinari. 1984. Empirical relation between electrical transverse resistance and hydraulic transmissivity. *Geoexploration* 22, no. 1: 1–15.

Purvance, D.T., and R. Andricevic. 2000. On the electrical-hydraulic conductivity correlation in aquifers. *Water Resources Research* 36, no. 10: 2905–2913.

Rehfeldt, K.R., J.M. Boggs, and L.W. Gelhar. 1992. Field study of dispersion in a heterogeneous aquifer. 3: Geostatistical analysis of hydraulic conductivity. *Water Resources Research* 28, no. 12: 3309–3324.

Sasaki, Y. 1992. Resolution of resistivity tomography inferred from numerical simulation. *Geophysical Prospecting* 40, 453–464.

Sturm, D.J. 2000. Experimental and field assessment of the dual domain model for describing solute transport in

heterogeneous media. Ph.D. diss., Department of Geology, University of Alabama.

Sudicky, E.A. 1986. A natural gradient experiment on solute transport in a sand aquifer: Spatial variability of hydraulic conductivity and its role on the dispersion process. *Water Resources Research* 22, no. 13: 2069–2082.

Tereschuk, T.A. 1998. Direct and statistical analysis of the effects of filtering and processing on ground penetrating radar data at the MADE Tracer Site, Columbus, Mississippi. M.S. thesis, Department of Geological and Mining Engineering and Sciences, Michigan Technological University.

Urish, D.W. 1981. Electrical resistivity-hydraulic conductivity relationships in glacial outwash aquifers. *Water Resources Research* 17, no. 5: 1401–1408.

Yeh, T.-C.J., S. Liu, R.J. Glass, K. Baker, J.R. Brainard, D. Alumbaugh, and D. LaBrecque. 2002. A geostatistically based inverse model for electrical resistivity surveys and its applications to vadose zone hydrology. *Water Resources Research* 38, no. 12: 14-1–14-13.

Yilmaz, O. 1987. *Seismic Data Processing*. Society of Exploration Geophysicists. Tulsa, OK.